Icarus 226 (2013) 945–950

Contents lists available at ScienceDirect

Icarus

journal homepage: www.elsevier.com/locate/icarus

Photolysis of H_2O–H_2O_2 mixtures: The destruction of H_2O_2

M.J. Loeffler [a,b,*], M. Fama [b], R.A. Baragiola [b], R.W. Carlson [c]

[a] NASA, GSFC, Astrochemistry Laboratory, Code 691, Greenbelt, MD 20771, United States
[b] University of Virginia, Laboratory for Atomic and Surface Physics, Charlottesville, VA 22904, United States
[c] Jet Propulsion Laboratory, California Institute of Technology, Pasadena, CA 91109, United States

ARTICLE INFO

Article history:
Received 15 March 2013
Revised 11 June 2013
Accepted 24 June 2013
Available online 16 July 2013

Keywords:
Europa
Ices, IR spectroscopy
Jupiter, satellites
Saturn, satellites
Photochemistry

ABSTRACT

We present laboratory results on the loss of H_2O_2 in solid $H_2O + H_2O_2$ mixtures at temperatures between 21 and 145 K initiated by UV photolysis (193 nm). Using infrared spectroscopy and microbalance gravimetry, we measured the decrease of the 3.5 μm infrared absorption band during UV irradiation and obtained a photodestruction cross section that varies with temperature, being lowest at 70 K. We use our results, along with our previously measured H_2O_2 production rates via ionizing radiation and ion energy fluxes from the spacecraft to compare H_2O_2 creation and destruction at icy satellites by ions from their planetary magnetosphere and from solar UV photons. We conclude that, in many cases, H_2O_2 is not observed on icy satellite surfaces because the H_2O_2 photodestruction rate is much higher than the production rate via energetic particles, effectively keeping the H_2O_2 infrared signature at or below the noise level.

Published by Elsevier Inc.

1. Introduction

Surfaces of most icy bodies in the outer Solar System and interstellar space are constantly bombarded with energetic particles and photons. Radiolytic products from these impacts can be detected from Earth and spacecraft by comparison of features in their reflectance spectra with those obtained in the laboratory. Some of our more recent laboratory studies using radiolysis to simulate the space environment (Loeffler et al., 2006a,b; Raut et al., 2012) have been motivated by the detection of H_2O_2 on Europa (Carlson et al., 1999), the lack of or lower than expected abundance of NH_3 detected on the surface of many saturnian icy satellites, such as Enceladus (Brown et al., 2006; Verbiscer et al., 2006), and the higher than expected CO_2:CO ratio found in the interstellar medium (Whittet et al., 1998).

In the work we report here, we have investigated the stability of H_2O_2 mixed in H_2O–ice when it is photolyzed with longer wavelength UV photons (>180 nm), which are weakly absorbed by H_2O. Our previous work on H_2O_2 was initially motivated by the detection of the 3.5 μm absorption band on the surface of Europa by the Galileo Near-Infrared Mapping Spectrometer (NIMS) (Carlson et al., 1999; Hansen and McCord, 2008). More recent ground-based studies have confirmed the NIMS results and have shown that there is nearly an order of magnitude more H_2O_2 in Europa's leading hemisphere than in its trailing hemisphere (Hand and Brown, 2013). The presence of H_2O_2 on Europa's surface, predicted by Johnson and Quickenden (1997), is not too surprising given that this satellite is subject to a high radiation flux (Cooper et al., 2001) and is mostly composed of water ice, a combination of which has long ago been shown to lead to H_2O_2 production (Ghormley and Stewart, 1956). Soon after the discovery of H_2O_2 on Europa, multiple laboratories verified that under relevant experimental conditions H_2O_2 could indeed be formed via radiolysis of water ice (Moore and Hudson, 2000; Gomis et al., 2004; Loeffler et al., 2006b; Zheng et al., 2006; Hand and Carlson, 2011). Unlike former studies, these radiolysis measurements were made *in situ* at the irradiation temperature studied, ensuring that the H_2O_2 detected was from irradiation and not from thermal reactions that may occur during warming. Although the amount estimated on Europa and in the laboratory was <1% with respect to H_2O, the strength and location of the absorption band made it seem likely that the NIMS detection on Europa would be the first of many on solid icy surfaces. However, new detections of condensed H_2O_2 on other surfaces have not been forthcoming, as the only other possible detection of H_2O_2 (Newman et al., 2007) on the icy satellite Enceladus has been disputed (Hodyss et al., 2009; Loeffler and Baragiola, 2009). Interestingly, Ganymede and Callisto, two other jovian satellites similar in composition and surface temperature to Europa but with lower radiation flux, have shown a slope in their ultraviolet reflectance spectra that is suggestive of H_2O_2 (Hendrix et al., 1999) yet no infrared absorption feature near 3.5 μm absorption region has been detected.

It is important to note that while Europa's surface is the only one in outer space where condensed H_2O_2 has been unequivocally

* Corresponding author at: NASA, GSFC, Astrochemistry Laboratory, Code 691, Greenbelt, MD 20771, United States.
E-mail address: mark.loeffler@nasa.gov (M.J. Loeffler).

0019-1035/$ - see front matter Published by Elsevier Inc.
http://dx.doi.org/10.1016/j.icarus.2013.06.030

detected, there have been a few gas phase detections of H_2O_2. For instance, H_2O_2 has been detected in Mars' atmosphere using both submillimeter (Clancy et al., 2004) and infrared spectroscopy (Encrenaz et al., 2004). Interestingly, the abundance of H_2O_2 in the martian atmosphere appears to have a time dependence, as these values were three to six times higher than previous upper limits provided estimated infrared spectroscopy (Encrenaz et al., 2002). This temporal dependence is also supported by more recent measurements by the Herschel telescope, which has not been able to observe H_2O_2 up to the previous detected levels (Hartogh et al., 2010). Most recently, using submillimeter spectroscopy gas phase H_2O_2 has been detected in the interstellar medium (Bergman et al., 2011), where solid H_2O_2 has been predicted to exist (Tielens and Hagen, 1982) but has yet to be detected.

The paucity of definitive H_2O_2 detections in outer space, especially in the solid phase, contrasted with its relative ease to produce and detect in the laboratory has led us to begin investigating possible mechanisms that could preferentially destroy H_2O_2 throughout the detection depth of the icy satellite surfaces (ten's of microns for the 3.5 μm band). Recent laboratory studies show that one possibility for the absence of H_2O_2 on Ganymede, Callisto and the trailing hemisphere of Europa is that this molecule may be consumed by thermally-induced reactions with contaminants in the ice, such as SO_2 (Loeffler and Hudson, 2013). Another likely mechanism, which is likely active in both pure and contaminated ice, is that the hydrogen peroxide may be efficiently destroyed by longer wavelength UV photons (>180 nm), which are weakly absorbed by water (>2 cm absorption length, Warren and Brandt, 2008) and can thus penetrate deeply into the surface ice. To test this possibility, we have photolyzed low concentrations of H_2O_2 in solid H_2O mixtures with UV photons (193 nm) at temperatures between 21 and 145 K. During photolysis, we have measured the photodestruction of H_2O_2 by monitoring the decrease of the 3.5 μm band with infrared spectroscopy and the photodesorption of the sample by monitoring the mass loss of our sample with our quartz crystal microbalance. Finally, we have extrapolated our photodestruction results to estimate the timescale on which this mechanism would be active on multiple surfaces in outer space.

2. Experimental details

All experiments were performed inside a cryopumped stainless-steel vacuum chamber on a radiation-shielded cryostat (see Loeffler et al., 2006c). The base pressure of the chamber was $\sim 3 \times 10^{-10}$ Torr and 1–2 orders of magnitude lower inside the shield. Solid hydrogen peroxide–water films were vapor deposited at 110 K onto an optically flat gold mirror electrode of a 6-MHz quartz-crystal microbalance (QCM). The areal mass (mass/area) of the films was determined (153 μg/cm^2–2 μm) by the change in the resonance frequency of the crystal, which was measured with an Inficon IC/5 controller to a resolution of 0.1 Hz (Sack and Baragiola, 1993). The measured areal mass can be converted to film column density η (molecules/cm^2) if the film composition is known, and converted to thickness if the mass density is known (Sack and Baragiola, 1993).

The H_2O–H_2O_2 mixtures were grown from a liquid solution of hydrogen peroxide and water using a glass doser (Loeffler and Baragiola, 2011). Each film contained between 0.5% and 2% H_2O_2, which was calculated from the band area of the infrared H_2O_2 absorption band at 3.5 μm, using previously calibrated band strengths at the same thickness (Loeffler et al., 2006b). After growth, samples were annealed to 135 K to allow diffusion to form the thermodynamically stable dihydrate diluted in water instead of clusters of hydrogen peroxide (Loeffler and Baragiola, 2005). After warming to 135 K, the samples were subsequently taken to the temperature where they were irradiated: 21–145 K.

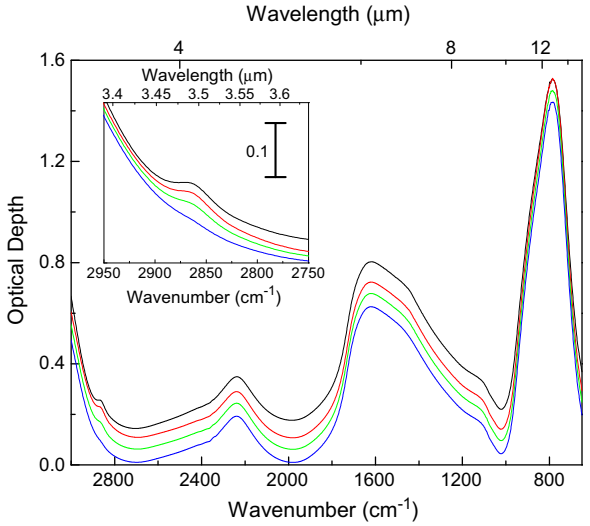

Fig. 1. Infrared spectrum of an $H_2O + H_2O_2$ mixture photolyzed at 100 K with 193 nm photons. Spectra from top to bottom at 2850 cm^{-1} is after 0, 1.6, 6.3, and 50×10^{19} photons/cm^2. The spectra have been offset vertically for clarity. The caption focuses in on the 3.5 μm absorption band of H_2O_2.

Irradiation was performed at normal incidence using a GAM ArF excimer laser (193 nm; 10 ns pulse width). The laser beam was defocused using a MgF_2 lens (f = 50 cm) to cover a rectangular spot ~25 mm × 75 mm at the target, larger than the active diameter of the microbalance (6 mm) to avoid multi-photon excitations or heating during each laser pulse. To measure the photon fluence reaching the target, we replaced the QCM with an Ophir power meter, which measured constant beam intensity across the area of the QCM. In these experiments, we measured that the laser delivered pulses of 1.2×10^{15} photons/cm^2/pulse uniformly across the films at a rate that we varied from 2 to 16 Hz during the experiment. The values of fluence are calculated taking into account the ~20% light reflected by the gold substrate (Canfield et al., 1964).

In addition to microbalance gravimetry, *in situ* characterization of our films was performed using infrared spectroscopy. The infrared specular reflectance between 1.5 and 15 μm was measured at an incident angle of 35° using a Thermo-Nicolet Nexus 670 Fourier Transform infrared spectrometer at 2-cm^{-1} resolution. The spectra were divided by the reflectance of the gold mirror substrate taken before film deposition and converted into absorption by taking the natural logarithm.

To quantify the column density of hydrogen peroxide present in the sample, we have typically calculated the band area of the infrared absorption feature at 3.5 μm by subtracting a non-linear continuum from the spectrum in optical depth units (Loeffler et al., 2006b). However, as is seen in Fig. 1, the H_2O_2 absorption band is very weak at high fluences, and thus here we analyze the derivative of the optical depth (−ln reflectance) spectrum. Fig. 2 shows that the absorption feature is more pronounced in the derivative, making quantification of small values (high fluences) more accurate. As the H_2O_2 absorption band does not change shape as it attenuates during photolysis, analysis using the band area or the derivative peak height yielded the same results within 5% over the region where a band area could be accurately calculated. Thus, data shown here will be given as the normalized peak-to-peak height of the derivative, which is obtained after subtracting the continuum baseline.

3. Results

Fig. 1 shows the infrared spectrum of our $H_2O + H_2O_2$ mixture before, during and after UV photolysis at 100 K between 3000 and

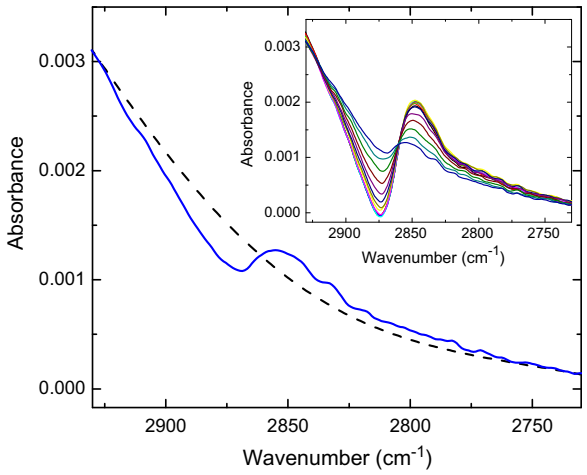

Fig. 2. Example of the derivative spectrum (solid curve) and the featureless continuum fit used (dashed curve) for a $H_2O + H_2O_2$ mixture after being photolyzed with 50×10^{19} photons/cm^2 at 100 K. Inset: all derivative spectra taken during photolysis at 100 K; the derivative peak to peak height decreases as the H_2O_2 in the sample decreases.

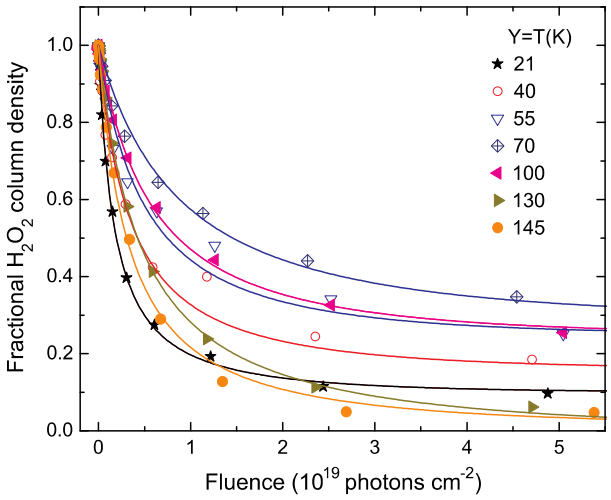

Fig. 3. Destruction of H_2O_2 in a $H_2O + H_2O_2$ mixture photolyzed at different temperatures. The solid line is a fit to the experimental data using Eq. (7). The curves tend asymptotically to a constant value. At the two higher temperatures the value cannot be distinguished from zero within fitting errors.

650 cm^{-1}. The spectra are dominated by the broad absorption bands of H_2O: $3\nu_L$ (2243 cm^{-1}), ν_2 (1621 cm^{-1}), and ν_L (780 cm^{-1}) and a weaker absorption band for ν_2 absorption band (2860 cm^{-1}) of H_2O_2. Photolysis has no clear effect on the water absorption bands, as expected since the absorption coefficient of H_2O at the wavelength of our laser (193 nm) is 0.159 m^{-1} (Warren and Brandt, 2008), and thus only ~0.00003% of light is absorbed by H_2O. Unlike water, the absorption band of H_2O_2 decreases during photolysis. However, no new absorption bands, such as those of HO_2 or HO_3, reported at 1142 cm^{-1} and 1259 cm^{-1} respectively (Cooper et al., 2006), are detected above the noise level in the spectra shown here or any of the other temperatures studied, which is likely due to the low level of H_2O_2 in the samples. Finally, we note that the general trends seen here were also observed when we photolyzed our sample with a broad band Hg lamp.

To quantify the photodestruction of H_2O_2, we analyzed the peak-to-peak of the derivative of the 2860 cm^{-1} absorption band of H_2O_2 during photolysis. The normalized results for all the temperatures studied are shown in Fig. 3. In all cases, the H_2O_2 decreases with laser fluence and continues to decrease at the highest doses used in this experiment. Interestingly, the rate of H_2O_2 destruction appears to be highest at the lowest temperature, consistent with radiolysis studies on $H_2O_2 + H_2O$ mixtures (Hudson and Moore, 2006) at 19 and 80 K. However, as the temperature is increased above 70 K, the destruction rate of H_2O_2 also increases. From Fig. 3, we can determine the fluence needed to destroy half of the H_2O_2 in the sample, $F_{1/2}$, and have shown these values in Table 1. One can see from Table 1 that the range of calculated $F_{1/2}$ varies significantly; the slowest decay (70 K) is ~9 times slower than at 21 K but only ~5 times lower at 145 K.

In addition to infrared spectroscopy, we also used our microbalance to estimate the photodesorption of our sample at $T \leqslant 130$ K, where thermal sublimation of H_2O is negligible. Assuming the mass loss is entirely due to H_2O_2, we estimate the yield to be ~1–4 $\times 10^{-5}$ H_2O_2/photon. Comparing these values to $F_{1/2}$ given in Table 1, we estimate that at most only about 3% of the H_2O_2 in the sample would be lost due to photodesorption by $F_{1/2}$, suggesting that the decrease in the infrared band area observed (such as in Fig. 1) is due to photodestruction and not photodesorption. Thus, the lack of detected decomposition products in Fig. 1 is likely a combination of the initial low H_2O_2 concentration in the sample and the fact that the infrared signal from the main decomposition product, OH (see Section 4), is masked by the OH stretch absorption from the water matrix.

Table 1
Fluence (10^{18} photons/cm^2) to reach $N = 0.5$ during photolysis of $H_2O_2 + H_2O$ mixtures.

T (K)	$H_2O_2 + H_2O$
145	3.2
130	4.4
100	9.9
70	17
55	11
40	5.0
21	1.9

4. Discussion

That solar light decomposes hydrogen peroxide has been known for more than a century (Downes and Blunt, 1877). Most studies since have been done in liquid aqueous solutions or in the gas phase. The few studies of radiation effects in frozen aqueous solutions of H_2O_2 done at temperatures relevant to the outer Solar System, have focused on the analysis of the electron paramagnetic resonance spectra of OH and HO_2 radicals, e.g., Wyard et al. (1968), Harrison and Symons (1993), and Beine and Anastasio (2011). Several interesting experiments have been performed with H_2O_2 isolated in rare gas matrices (e.g., Khriachtchev et al. (2000)), but the absence of the hydrogen-bonded matrix would make questionable a translation of those results to our case. Rather, to explain our data, we will base the majority of our discussion on what has been learned from studies performed in the gas phase, keeping in mind the difference in solid vs. gas phase reactions, namely the higher probability of radical recombination due to the presence of a lattice.

4.1. Photolysis pathways

First, as we observe no apparent changes in H_2O infrared absorption bands during photolysis (Fig. 1) and note that H_2O is essentially transparent to the 193 nm light, we neglect the initial role of water and consider only photoabsorption by H_2O_2.

Photoabsorption at 193 nm occurs with a cross section (in cm^2-molecule^{-1}) of $\sigma_a = 6 \times 10^{-19}$ (vapor) and 1.26×10^{-18} (liquid solution) (Lin et al., 1978) and leads to dissociation (Bersohn and Shapiro, 1986), which is confirmed by a total quantum yield for dissociation near unity (Vaghjiani et al., 1992). Photoabsorption promotes an oxygen lone pair to an anti-bonding orbital, leading to the scission of the weak (2.15 eV) O–O bond, with two ground-state and vibrationally unexcited hydroxyl fragments rotating in opposite sense around the O–O axis (Grunewald et al., 1986). Alternatively, the H–OOH bond may be broken, leading to a H atom and HO_2 (Gerlach-Meyer et al., 1987), as in (2) below:

$$h\nu + H_2O_2 \rightarrow OH + OH + 4.3\ \text{eV} \quad (80\%) \tag{1}$$

$$h\nu + H_2O_2 \rightarrow HO_2 + H + 2.5\ \text{eV} \quad (20\%) \tag{2}$$

The relative importance of each of these outcomes, and the absence of a significant O-atom product have been established by several later studies (Vaghjiani et al., 1992; Schiffman et al., 1993; Nakayama et al., 2005).

In the condensed state, the dissociation cross-section σ is lower than the absorption cross-section σ_a because of the cage effect. Dissociation products collide with the cage of molecules surrounding the excited molecule and can return to reform hydrogen peroxide by the exothermal reactions $OH + OH \rightarrow H_2O_2$ and $H + HO_2 \rightarrow H_2O_2$. As a result, the quantum yield $\Phi = \sigma/\sigma_a < 1$. This is likely the reason why Φ is seen to drop from 1.6 OH/photon in the gas phase to 0.7 OH/photon in the condensed phase (Chu and Anastasio, 2005).

As the fluence of photons increases, reaction products accumulate in the sample and secondary reactions can occur if the initial H_2O_2 concentration is sufficiently high and diffusion allows collisions involving radicals, which occurs at higher temperatures, more than about 100 K. In addition, the 193 nm photons can dissociate some products. The photoabsorption cross sections for gas phase HO_2 is 4×10^{-18} cm^2 (Sander et al., 2006), or approximately seven times higher than gas phase H_2O_2, while photoabsorption by OH, OH, O_2 and H_2 are negligible compared to that of H_2O_2.

Of the main reaction products given in (1) and (2), only HO_2 could possibly be detected in our sample, as the OH is masked by the H_2O and the H atom will not have a detectable infrared signature. However, no HO_2 is observed in the infrared 1142 cm^{-1} during any point in photolysis at all temperatures studied. Thus for the point of modeling our results, we assume that (1) is the dominant destruction pathway, and thus the only secondary reaction that may be important is the reformation of H_2O_2 via OH recombination. Thus, we write the dependence of the hydrogen peroxide concentration $[H_2O_2]$ with time t as:

$$d[H_2O_2]/dt = -\phi\sigma[H_2O_2] + \phi\sigma[H_2O_2]k[OH] \tag{3}$$

where ϕ is the photon flux, σ is the destruction cross-section for H_2O_2, and k is a measure of the reaction area of OH radicals that results in the formation of H_2O_2 (rather than $H_2O + O$, see reactions (11) and (12) below). The second term, valid in the absence of OH diffusion, describes the probability that dissociation occurs near the location of a previously formed OH and, hence, is appropriate below about 110–120 K. Here we are assuming that [OH] is always small and therefore neglect radical recombination when the light is off, and thus the only way H_2O_2 can reform is if one H_2O_2 molecule is photolyzed near a trapped OH. By multiplying by the film thickness L we can express Eq. (3) in terms of column densities P and H (for peroxide and hydroxyl, respectively). Writing the fluence differential as $F = \phi dt$ and $c = kL$, we can rewrite (3) as:

$$dP/dF = -\sigma P + \sigma PcH \tag{4}$$

Since two hydroxyls form every time hydrogen peroxide is destroyed, we can relate the two molecules by the following relation:

$$P = H = 2[P_0 - P] \tag{5}$$

where P_0 is the initial column density of hydrogen peroxide. We then can rewrite (5) in terms of only the hydrogen peroxide column density:

$$dP/dF = -\sigma P + \sigma P2c[P_0 - P] = -\sigma P(1 - 2cP_0) - 2c\sigma P^2 \tag{6}$$

We can integrate (11) to obtain:

$$\frac{P}{P_0} = \frac{a}{(a+b)e^{aF} - b} \tag{7}$$

$$a = \sigma[1 - 2cP_0]; \quad b = 2c\sigma P_0 \tag{8}$$

Fig. 3 shows the least square fits of Eq. (7) to the experimental data. The closeness of the fit to the data supports our assumption that the primary decomposition product is OH and that H_2O_2 can be reformed by hydroxyl recombination. The net destruction cross section measured at each temperature is shown in Fig. 4. It starts with an initial high value at 21 K and drops but begins to increase above ~100 K, at the onset of OH diffusion in ice (Kroh et al., 1962). Radical mobility allows for interaction of radicals and further hydrogen peroxide destruction by the Haber–Weiss chain reaction (Lunak and Sedlak, 1992):

$$OH + H_2O_2 \rightarrow HO_2 + H_2O \tag{9}$$

$$HO_2 + H_2O_2 \rightarrow OH + H_2O + O_2 \tag{10}$$

which can be terminated by a number of reactions that destroy OH, such as

$$2OH \rightarrow H_2O_2 \tag{11}$$

$$2OH \rightarrow H_2O + O \tag{12}$$

The O atom produced in reaction (13) may be important for the production of other secondary products, such as O_2 or O_3, yet none of these are observed in our sample.

4.2. Astrophysical implications

To calculate the effect of solar irradiation on the jovian icy satellites we need to integrate the product of the solar flux and the destruction cross section along the wavelength spectrum. The solar flux at these satellites is obtained from the irradiance measured by the UARS probe outside the Earth's atmosphere (Woods et al., 1996) on 29 March 1992 scaled out to the 5.2 AU distance of the

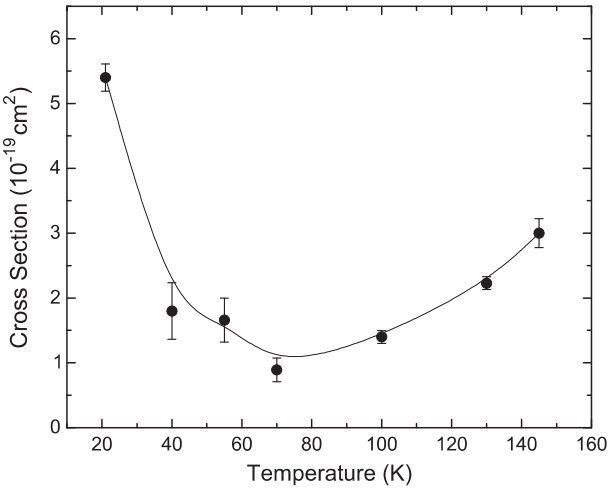

Fig. 4. Photodestruction cross section for the $H_2O + H_2O_2$ mixture as a function of temperature.

jovian system by dividing by the square of the distance. To arrive at the destruction cross section, we first calculate the photoabsorption rate as the integral of the photon flux and the absorption cross section σ_a, given by Lin et al. (1978) above 189 nm for aqueous solutions and by Suto and Lee (1983) for gaseous H_2O_2 below 193 nm; we multiplied the Suto and Lee data by a factor of two to match the aqueous solution data. Fig. 5 shows the solar flux at the jovian satellites, the photoabsorption cross-section, and the differential absorption rate per nm. The integral of the latter curve gives an absorption rate of $7 \times 10^{-6}\ s^{-1}$ at the subsolar point.

To obtain the photodestruction rate, the absorption rate needs to be multiplied by the quantum yield for dissociation, Φ, which is less than 1 due to the cage effect. It is given by the ratio of our photodestruction cross section (Fig. 5) and the photoabsorption cross section of $1.3 \times 10^{-18}\ cm^{-2}$ at 193 nm (Lin et al., 1978). For an average equatorial temperature of 106 K appropriate to Europa (Spencer et al., 1999), $\Phi \sim 0.1$. Assuming that Φ does not vary much with wavelength, as happens for room temperature solutions between 205 and 400 nm (Goldstein et al., 2007), the initial (zero fluence) photodestruction rate at Europa at the subsolar point is $7 \times 10^{-7}\ s^{-1}$. Considering that the total flux on the surface of the satellite is ¼ the solar flux, we obtain a global mean photodestruction rate of $1.8 \times 10^{-7}\ s^{-1}$, averaged over time and latitude, implying a lifetime of ~1500 h. Variations of solar activity and the eccentricity of Jupiter's orbit will cause temporal changes of ~40% in the rates (Woods and Rottman, 2002), while variations due to temperature between high and low latitudes should be much smaller, as judged from our data of Fig. 5.

4.3. Comparison with charged particle irradiation

The amount of hydrogen peroxide in water ice at Europa and other icy satellites is given by the competition between the formation rate (mostly by charged magnetospheric particles) and the destruction rate by particles and solar UV. The photolytic production of H_2O_2 from water is negligible since it requires wavelengths shorter than ~160 nm, where the solar flux is small and, even for Lyman-α the equilibrium column density formed can be calculated to be $\sim 4 \times 10^{15}\ cm^{-2}$ from photochemistry experiments at 10 K (Gerakines et al., 1996) using 5.7×10^{-17} cm molecule^{-1} for the strength of the 3.5 μm absorption band (Loeffler et al., 2006b). Such column density is 20–400 times smaller than the estimated value at Europa (Carlson et al., 1999) and limited to the shallow penetration depth of Lyman-α (~40 nm).

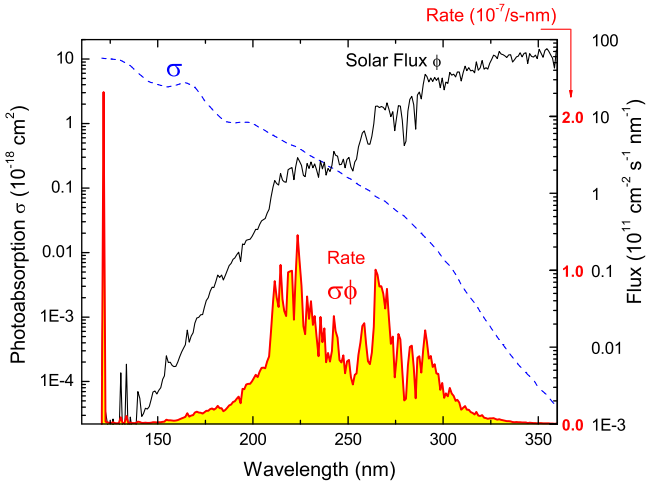

Fig. 5. Black line: Solar flux at subsolar surface on the jovian satellites calculated from the flux outside Earth obtained by Woods et al. (1996) on March 29, 1992. Dashed blue line: photoabsorption cross section of H_2O_2 in water from Lin et al. (1978) (above 189 nm) and from Suto and Lee for the gas phase (below 193 nm) multiplied by 2 to fit the data of Lin et al. The product of the flux and the cross section, shown by the red line, is the differential photoabsorption flux per nm. The integral, yellow area, is the total subsolar photoabsorption rate of $7 \times 10^{-6}\ s^{-1}$. (For interpretation of the references to color in this figure legend, the reader is referred to the web version of this article.)

The formation of H_2O_2 by magnetospheric ions and electrons can be obtained by using a radiolytic yield, G (in molecules per 100 eV deposited): $G(H_2O_2) = 0.36$ for ions (Loeffler et al., 2006b) with high stopping power, and 0.028–0.051 for weakly ionizing 10 keV electrons at 80–100 K (Hand and Carlson, 2011). The sensitivity of H_2O_2 production to the density of energy deposition is discussed by Burns and Sims (1981) and Loeffler et al. (2006b). Using proton fluxes collected by Cooper et al. (2001) and $G(H_2O_2) = 0.36$, since the peak proton energy at Europa is ~100 keV (Paranicas et al., 2002) we obtain an areal H_2O_2 production rate (in units of $10^9\ cm^{-2}\ s^{-1}$) of 40 at Europa, 4 (0.1) at Ganymede's poles (equator), and 0.08 at Callisto. The variation among these satellites is determined by their proximity to Jupiter and the existence of a local magnetic field at Ganymede. We note that on all satellites the H_2O_2 production rate may be slightly higher as heavy ions and high energy electrons will also contribute to H_2O_2 production.

The destruction of H_2O_2 by magnetosphere protons at Europa was calculated by Loeffler et al. (2006b) as $8.9 \times 10^{-7}\ s^{-1}$, which is ~5 times higher than the global mean photodestruction rate calculated above. Thus, at Europa, the abundance of hydrogen peroxide is mainly determined by ion impacts. At the other jovian icy satellites, where particle fluxes and hence the H_2O_2 are much lower, photodestruction limits concentrations of hydrogen peroxide to much lower than the 0.0013 value for Europa's leading hemisphere, which may explain the absence of detection of this molecule on the other jovian satellites.

On Enceladus, as the energetic proton flux is very low (Paranicas et al., 2008), H_2O_2 production is likely dominated by energetic electrons, which are ~10 times less efficient in producing H_2O_2 than keV protons. Using an average G value of 0.04 (Hand and Carlson, 2011), we estimate that the areal H_2O_2 production rate from energetic electrons is $\sim 2 \times 10^8\ cm^{-2}\ s^{-1}$ for the nominal (averaged) flux given in Cooper et al. (2009), or about a factor of 200 lower than on Europa. Given that the solar flux would only be attenuated by a factor of 3.2, compared to the jovian satellites, we expect that the absence of H_2O_2 on Enceladus is likely due to the high efficiency of photodestruction.

Finally, due to the high transparency of water in the UV above 180 nm, solar irradiation will reach depths much deeper than where most radiolysis products are formed, effectively bleaching depths on the order of millimeters for those molecules that diffuse deeper in the ice. The photodestruction of H_2O_2 at greater depths (~cm), where higher energy electrons (~10 MeV) can form H_2O_2, is likely less important due to scattering caused by grains and absorption caused by other species mixed in the grains.

5. Conclusions

In this work, we have used infrared spectroscopy and microbalance gravimetry to study the photodecomposition by 193 nm photons of H_2O_2 in solid $H_2O_2 + H_2O$ mixtures at temperatures between 21 and 145 K. We find that the area of the 3.5 μm infrared absorption of H_2O_2 decreases with photon fluence at all temperatures studied, and that the destruction rate is slowest at 70 K. Microbalance gravimetry indicates that the loss of H_2O_2 observed in the infrared cannot be due to photodesorption and thus must be due to photodestruction of the H_2O_2. To quantify the photodestruction of H_2O_2, we developed a two-component model that adequately fits our data and yields a destruction cross section for each temperature studied.

Extrapolating our results to the icy satellites, we find that the presence of H_2O_2 on Europa is consistent with our results, as the photodestruction rate is lower than the average ion destruction rate. However, on Ganymede and Callisto, given that the photodestruction rate is essentially the same as it is on Europa and that the ion energy flux (and hence H_2O_2 production rate) is significantly lower, we conclude that the UV light will effectively lower the equilibrium concentration of H_2O_2 on the surface by at least a factor of five making H_2O_2 much more difficult to detect. Similarly on Enceladus we estimate that the H_2O_2 production rate is ~200 times lower than on Europa, and thus since the photodestruction rate is only about three times lower, we suggest that the absence of H_2O_2 on the surface of Enceladus is likely due to the high efficiency of photodestruction. Finally, given that the photodestruction of H_2O_2 clearly plays a role on determining its equilibrium concentration on the icy satellites, predicting what satellites will have H_2O_2 will come down to characterizing the ionizing radiation environment at the surface, as well as other factors such as the composition.

Acknowledgments

This work is being funded by NASA Outer Solar System Program. M. Loeffler thanks J. Cooper and P. Gerakines for useful discussions.

References

Beine, H., Anastasio, C., 2011. The photolysis of flash-frozen dilute hydrogen peroxide solutions. J. Geophys. Res. 116, D14302.
Bergman, P. et al., 2011. Detection of interstellar hydrogen peroxide. Astron. Astrophys. 531, L8 (4 pp).
Bersohn, R., Shapiro, M., 1986. Photodissociation dynamics and potential energy surfaces of hydrogen peroxide. J. Chem. Phys. 85, 1396–1402.
Brown, R.H. et al., 2006. Composition and physical properties of Enceladus' surface. Science 311, 1425–1428.
Burns, W.G., Sims, H.E., 1981. Effect of radiation type in water radiolysis. J. Chem. Soc. Faraday Trans. I 77, 2803–2813.
Canfield, L.R., Hass, G., Hunter, W.R., 1964. The optical properties of evaporated gold in the vacuum ultraviolet from 300 A to 2000 A. J. Phys. 25, 124–129.
Carlson, R.W. et al., 1999. Hydrogen peroxide on the surface of Europa. Science 283, 2062–2064.
Chu, L., Anastasio, C., 2005. Formation of hydroxyl radical from the photolysis of frozen hydrogen peroxide. J. Phys. Chem. A 109, 6264–6271.
Clancy, R.T., Sandor, B.J., Moriarty-Schieven, G.H., 2004. A measurement of the 362 GHz absorption line of Mars atmospheric H_2O_2. Icarus 168, 116–121.
Cooper, J.F., Johnson, R.E., Mauk, B.H., Garrett, H.B., Gehrels, N., 2001. Energetic ion and electron irradiation of the icy Galilean satellites. Icarus 149, 133–159.
Cooper, P.D., Moore, M.H., Hudson, R.L., 2006. Infrared detection of HO_2 and HO_3 radicals in water ice. J. Phys. Chem. A 110, 7985–7988.
Cooper, J.F., Cooper, P.D., Sittler, E.C., Sturner, S.J., Rymer, A.M., 2009. Old faithful model for radiolytic gas-driven cryovolcanism at Enceladus. Planet. Space Sci. 57, 1607–1620.
Downes, A., Blunt, T.P., 1877. Researches on the effect of light upon bacteria and other organisms. Proc. R. Soc. 28, 488–500.
Encrenaz, T. et al., 2002. A stringent upper limit of the H_2O_2 abundance in the martian atmosphere. Astron. Astrophys. 396, 1037–1044.
Encrenaz, T. et al., 2004. Hydrogen peroxide on Mars: Evidence for spatial and seasonal variations. Icarus 170, 424–429.
Gerakines, P.A., Schutte, W.A., Ehrenfreund, P., 1996. Ultraviolet processing of interstellar ice analogs. I. Pure ices. Astron. Astrophys. 312, 289–305.
Gerlach-Meyer, U., Linnebach, E., Kleinermanns, K., Wolfrum, J., 1987. H-atom photofragments from H_2O_2 dissociated at 193 nm. Chem. Phys. Lett. 133, 113–115.
Ghormley, J.A., Stewart, A.C., 1956. J. Am. Chem. Soc. 78, 2934–2939.
Goldstein, S., Aschengrau, D., Diamant, Y., Rabani, J., 2007. Photolysis of aqueous H_2O_2: Quantum yield and applications for polychromatic UV actinometry in photoreactors. Environ. Sci. Technol. 41, 7486–7490.
Gomis, O., Satorre, M.A., Strazzulla, G., Leto, G., 2004. Hydrogen peroxide formation by ion implantation in water ice and its relevance to the Galilean satellites. Planet. Space Sci. 52, 371–378.
Grunewald, A.U., Gericke, K.-H., Comes, F.J., 1986. Photofragmentation dynamics of H_2O_2 at 193 nm. Chem. Phys. Lett. 132, 121–127.
Hand, K.P., Brown, M.E., 2013. Keck II observations of hemispherical differences in H_2O_2 on Europa. Astrophys. J. Lett. 766, L21 (4pp).
Hand, K.P., Carlson, R.W., 2011. H_2O_2 production by high-energy electrons on icy satellites as a function of surface temperature and electron flux. Icarus 215, 226–233.
Hansen, G.B., McCord, T., 2008. Widespread CO_2 and other non-ice compounds on the anti-jovian and trailing sides of Europa from Galileo/NIMS observations. Geophys. Res. Lett. 35, L01202.
Harrison, N., Symons, M.C.R., 1993. Detection of radical pairs in glassy systems. J. Chem. Soc. Faraday Trans. I 89, 59–61.
Hartogh, P. et al., 2010. Herschel/HIFI observations of Mars: First detection of O_2 at submillimetre wavelengths and upper limits on HCl and H_2O_2. Astron. Astrophys. 521, L49 (5 pp).
Hendrix, A.R., Barth, C.A., Stewart, A.I.F., Hord, C.W., Lane, A.L., 1999. Hydrogen peroxide on the icy Galilean satellites. Lunar Planet. Sci. 30. Abstract 2043.
Hodyss, R. et al., 2009. Methanol on Enceladus. Geophys. Res. Lett. 36, L17103 (3 pp).
Hudson, R.L., Moore, M.H., 2006. Infrared spectra and radiation stability of H_2O_2 ices relevant to Europa. Astrobiology 6, 483–489.
Johnson, R.E., Quickenden, T.I., 1997. Photolysis and radiolysis of water ice in outer Solar System bodies. J. Geophys. Res. 102, 10985–10996.
Khriachtchev, L., Pettersson, M., Jolkkonen, S., Pehkonen, S., Rasanen, M., 2000. Photochemistry of hydrogen peroxide in Kr and Xe matrixes. J. Chem. Phys. 112, 2187–2194.
Kroh, J., Green, B.C., Spinks, J.W.T., 1962. Electron paramagnetic resonance studies of free radicals produced by Tβ-particles in frozen H_2O and D_2O media at liquid nitrogen temperature. Can. J. Chem. 40, 413–425.
Lin, C.L., Rohatgi, N.K., DeMore, W.B., 1978. Ultraviolet absorption cross sections of hydrogen peroxide. Geophys. Res. Lett. 5, 113–115.
Loeffler, M.J., Baragiola, R.A., 2005. The state of hydrogen peroxide on Europa. Geophys. Res. Lett. 32, 17202 (4 pp).
Loeffler, M.J., Baragiola, R.A., 2009. Is the 3.5 μm infrared feature on Enceladus due to hydrogen peroxide? Astrophys. J. 694, L92–L94.
Loeffler, M.J., Baragiola, R.A., 2011. Isothermal decomposition of hydrogen peroxide dihydrate. J. Phys. Chem. A 15, 5324–5328.
Loeffler, M.J., Hudson, R.L., 2013. Low-temperature thermal reactions between SO_2 and H_2O_2 and their relevance to the jovian icy satellites. Icarus 224, 257–259.
Loeffler, M.J., Raut, U., Baragiola, R.A., 2006a. Enceladus: A source of nitrogen and an explanation for the water vapor plume observed by CASSINI. Astrophys. J. 649, L133–L136.
Loeffler, M.J., Raut, U., Vidal, R.A., Baragiola, R.A., Carlson, R.W., 2006b. Synthesis of hydrogen peroxide in water ice by ion irradiation. Icarus 180, 265–273.
Loeffler, M.J., Teolis, B.D., Baragiola, R.A., 2006c. Decomposition of solid amorphous hydrogen peroxide by ion irradiation. J. Chem. Phys. 124, 104702 (6 pp).
Lunak, S., Sedlak, P., 1992. Photoinitiated reactions of hydrogen-peroxide in the liquid-phase. J. Photochem. Photobiol. A: Chem. 68, 1–33.
Moore, M.H., Hudson, R.L., 2000. IR detection of H_2O_2 at 80 K in ion-irradiated laboratory ices relevant to Europa. Icarus 145, 282–288.
Nakayama, T., Takahashi, K., Matsumi, Y., 2005. Quantum yield for hydrogen atom formation from H_2O_2 photolysis in the range 193–240 nm. Int. J. Chem. Kinet. 37, 751–754.
Newman, S.F., Buratti, B.J., Jaumann, R., Bauer, J.M., Momary, T.W., 2007. Hydrogen peroxide on Enceladus. Astrophys. J. 670, L143–L146.
Paranicas, C., Ratliff, J.M., Mauk, B.H., Cohen, C., Johnson, R.E., 2002. The ion environment near Europa and its role in surface energetics. Geophys. Res. Lett. 29, 18 (4 pp).
Paranicas, C. et al., 2008. Sources and losses of energetic protons in Saturn's magnetosphere. Icarus 197, 519–525.
Raut, U., Fulvio, D., Loeffler, M.J., Baragiola, R.A., 2012. Radiation synthesis of carbon dioxide in ice-coated carbon: Implications for interstellar grains and icy moons. Astrophys. J. 752, 159 (8 pp).
Sack, N.J., Baragiola, R.A., 1993. Sublimation of vapor-deposited water ice below 170 K, and its dependence on growth conditions. Phys. Rev. B 48, 9973–9978.
Sander, S.P. et al., 2006. Chemical Kinetics and Photochemical Data for Use in Atmospheric Studies Evaluation Number 15, vol. 06-2. Jet Propulsion Laboratory.
Schiffman, A., Nelson Jr., D.D., Nesbitt, D.J., 1993. Quantum yields for OH production from 193 and 248 nm photolysis of HNO_3 and H_2O_2. J. Chem. Phys. 98, 6935–6946.
Spencer, J.R., Tamppari, L.K., Martin, T.Z., Travis, L.D., 1999. Temperatures on Europa from Galileo photopolarimeter–radiometer: Nighttime thermal anomalies. Science 284, 1514–1516.
Suto, M., Lee, L.C., 1983. $(OH)A^2\Sigma_+ \rightarrow X^2\Pi$ yield from photodissociation of H_2O_2 at 106–193 nm. Chem. Phys. Lett. 98, 152–156.
Tielens, A.G.G.M., Hagen, W., 1982. Model calculations of the molecular composition of interstellar grain mantles. Astron. Astrophys. 114, 245–260.
Vaghjiani, G.L., Turnipseed, A.A., Warren, R.F., Ravishankara, A.R., 1992. Photodissociation of H_2O_2 at 193 and 222 nm – Products and quantum yields. J. Chem. Phys. 96, 5878–5886.
Verbiscer, A.J. et al., 2006. Near-infrared spectra of the leading and trailing hemispheres of Enceladus. Icarus 182, 211–223.
Warren, S.G., Brandt, R.E., 2008. Optical constants of ice from the ultraviolet to the microwave. J. Geophys. Res. 113, D14220.
Whittet, D.C.B. et al., 1998. Detection of abundant CO_2 ice in the quiescent dark cloud medium toward Elias 16. Astrophys. J. 498, L159–L163.
Woods, T.N., Rottman, G., 2002. Solar ultraviolet variability over times of aeronomic interest. Geophys. Monogr. Ser. 230, 221–233.
Woods, T.N. et al., 1996. Validation of the UARS solar ultraviolet irradiances: Comparison with the ATLAS 1 and 2 measurements. J. Geophys. Res. 101, 9541–9589.
Wyard, S.J., Smith, R.C., Adrian, F.J., 1968. ESR spectrum of HO_2 in solutions of hydrogen peroxide in water at 77 K. J. Chem. Phys. 49, 2780–2783.
Zheng, W., Jewitt, D., Kaiser, R.I., 2006. Formation of hydrogen, oxygen, and hydrogen peroxide in electron-irradiated crystalline water ice. Astrophys. J. 639, 534–548.